

Generation and characteristic of internal tidal beam in Tasman Sea

September 24, 2017

Abstract

Macquarie Ridge south of New Zealand is a strong generator of internal tidal waves (ITs) which later form a prominent internal tidal beam, tight filament of baroclinic tidal energy. The mechanism of barotropic energy conversion into baroclinic field is investigated by means of numerical experiments with prescribed mesoscale conditions corresponding to different background conditions. The obtained energy transfer rates into IT mode-1 show variability both in its magnitude and spatial distribution. This variability is controlled by resonance between local barotropic forcing and remotely generated ITs. The remote baroclinic signal takes its origin at an easterly located Campbell Plateau. Their pathway is drastically different from the progressive plane waves due to interference with the ridge originating waves and consequent formation of a standing Poincare wave. This complex internal tide environment is modulated by the ratio of the respective East and West traveling components. *The west part associated with the plateau experiences variability following the upper ocean stratification. (this currently questionable)* Under conditions of the Tasman Sea subtropical frontal zone located northward of the region, leading to weaker stratification, lower amplitude waves, a more developed standing wave and hence, less energy transfer into the internal tidal beam. Conversely, under different realization an intrusion of warm subtropical waters created conditions for stronger generation resulting in high across Macquarie ridge energy transport and larger conversion rates. This mechanism of variability is further shown to affect position of the internal tidal beam. It is characterized by complex pattern of nodes and antinodes. The simple inverse analytical models shows that spatially wide-spread generation is one to blame. Than it is shown that the beam wobbles as a result in shifting of internal tide production hotspots. This identifies a reason for beam long range nonstationarity as a result of generation nonstationarity.

The inverse model based on elliptical waves shows that the beam undergoes changes in its appearance similar to Fresnel and Fraunhoffer diffraction in optics.

1 Introduction

Baroclinic semidiurnal tides originate as a strong barotropic flow occurs over steep topography in stratified ocean. This process is though as a scattering of barotropic tidal energy

into baroclinic motions (Wunsch (1975)). It is quite definitely known that the scattering has a large impact on energetics barotropic tide and is a part of energy dissipation (Egbert and Ray (2000), Munk (1997)) with 1/3 of M_2 energy being dissipated through generation of internal tide.

Analytical models of internal tide generation points to importance of ratio between direction of internal wave characteristics to bathymetry slope (Garrett and Kunze (2007)). Omitting nonlinear regimes for low Froude number flows, highly supercritical slopes will give rise mostly to the gravest mode of internal tide (Echeverri and Peacock (2010)). Such a case for Macquarie Ridge located south of New Zealand. Here barotropic tide energy is converse into largely mode-1 baroclinic tide.

Variability of internal tide generation can occur to number of reasons. Stratification could have a direct impact in WKB sense creating less prominent obstacle (Holloway and Merrifield (1999)). But this phenomena is more pronounced for bathymetry touching pycnocline. More recently, it became apparent that the generation is more unstable in presence of remote baroclinic signals. In the most well studied setting of two parallel ridges a resonance conditions occurs (Echeverri and Peacock (2010), Buijsman et al. (2012b), Buijsman et al. (2014)) that would lead either to intensification or destruction of energy transfers. More generally, phenomena of coupling at internal tide production sites of local generation and remote signal can lead to nonstationarity in wave generation (Kelly and Nash (2010), Osborne et al. (2011), Kerry et al. (2013), Xing and Davies (1998), Buijsman et al. (2012a)). The notion of variability in generation was observed as well (Pickering et al. (2015), Zilberman et al. (2011)). The same phenomena occurs at Macquarie Ridge where behind located Campbell Plateau sends internal tides which results in generation variability.

The ubiquitous feature of mode-1 internal tides as they leave production sites is their appearance as tightly confined beams of energy propagating without much spreading over large distances (Zhao et al. (2016)). This surprising feature is believed to be related to multiple generation sites (Rainville et al. (2010), Terker et al. (2014)). Especially, this is true for long swaths of generation bathymetry where point source two dimensional models of generation becomes unrealistic (Munroe and Lamb (2005)).

The question of stationarity of the tidal beams is still open. The most obvious reason for variations is variable mesoscale conditions in open sea (Kerry et al. (2016), Dunphy and Lamb (2014), Chavanne et al. (2010), Ansong et al. (2017), Dunphy et al. (2017), Zaron and Egbert (2014), ?). On the first order, Doppler shift by background currents and refraction by variable stratification is a key processes or reflection at strong frontal zones. Oppositely, here we will pursue different point such that variable spatial conversion rates will lead to reorganization of Tasman Sea tidal beam.

This is done by investigation of numerical experiments in Regional Ocean Modeling System with different realistic background conditions (Section 2). By deriving energy parameters it is shown that variations occur both at generation regions (Section 3a), but also in open ocean (Section 3b). Further analysis shows that remote signal is responsible for variations in Macquarie Ridge region (Section 4a) and than bridge to mid-basin characteristics by semi-analytical model (Section 4b) it is shown that generation is one to blame in nonstationarity (Section 4c). In conclusions we discuss how wide-spread this phenomena is (Section 5).

Conversion of bt to bc large scale picture: beams, nonspatial uniformity

Remote tides and local forcing: Sam, Carry

Resonance, Luzon Strait: : Echeverri, Buijsman, Pickering
Macquarie Ridge and Tasman Beam
Outline

2 Numerical experiments and analysis

2.1 Numerical experiments

It is used Regional Ocean Modeling System. The numerical domain covers southern Tasman Sea basin with grid spacing of $1/32^\circ$ and 50 vertical σ -levels. To simplify results M_2 -harmonic forced as boundary condition.

Several cases of different background conditions is considered (Table 1). In the simple setting no background conditions are prescribed with spatially uniform stratification representative of climatological mean. Other simulations were initialized with HYCOM hindcasted three dimensional fields of horizontal currents and stratification. On the boundaries the same fields were forced through simulation. On the top MERRA fields were given through insolation, air temperature, evaporation-precipitation rates and wind stresses. These parameters were taken for the given in table periods.

The simulation were sampled after 10 days of spin up that mode-1, 2 internal tide reached stationary behavior.

To outline scattering energetics additionally MITgcm simulation was done with similar background conditions as 'Uni' and same resolution.

The following analysis was carried on the last 5 day simulations. For the long run (2015_TBEAM) the output was sampled in 5 days non-overlapping windows.

2.2 Internal tide analysis

The output was highpassed (30 hours cutoff) with Butterworth filter to remove mesoscale signal. From isopycnal displacements baroclinic perturbation was found by imposing "barotropic" condition (? , ?),

$$p = \int_{-H}^0 \rho' dz.... \quad (1)$$

Such obtained currents and density perturbations were harmonically fit to M_2 period. The vertical structure functions were calculated for each grid point. The eigenmodes were than fit to find amplitudes of the first 3 modes. Than energetic properties of the wave field were found.

From the model output transfer of barotropic energy into mode-1 internal tide was diagnosed by

$$C_{bt, 1} = \frac{1}{T} \int_0^T \nabla \cdot \vec{u}_{bt} \cdot \tilde{p}_1 dt \quad (2)$$

Table 1: Carried out numerical experiments

Numerical experiments used in this study		
Experiment Name	Dates	Comments
Uni	NA	Homogeneous background conditions
2012	Janaury 1st - January 15th 2012	NA
2013	Janaury 1st - January 15th 2013	NA
2014	Janaury 1st - January 15th 2014	NA
2015	Janaury 1st - January 15th 2015	NA
2015_TBEAM	Janaury 1st - March 1st 2015	to cover field period
2013_274	DOY: 274 - 289 - 2013	to test generation hypothesis
2015_074	DOY: March 1st - March 15th 2015	to test generation hypothesis

with the first term representing barotropic forcing and second - mode-1 baroclinic pressure anomaly.

The energy flux was obtained from decomposed into barotropic and baroclinic signals (?) as

$$F = up \quad (3)$$

For MITgcm we calculated mode energy transfers to show reflection between Macquarie Ridge and Campbell plateau.

2.3 The simulated BT tide and TPXO?

3 Results

3.1 Beam and conversion: General outlook

Uniform: Three beams similar to satellite. Central primarily originates in main Macquarie Ridge. There is large variability in the northern, southern, but central is stable.

There two major generation hotspots associated with steep submarine seamounts (Figure 1).

The other region of generation is behind located Campbell Plateau.

Additionally, there is a standing wave. Now we investigate interaction between conversion and standing wave.

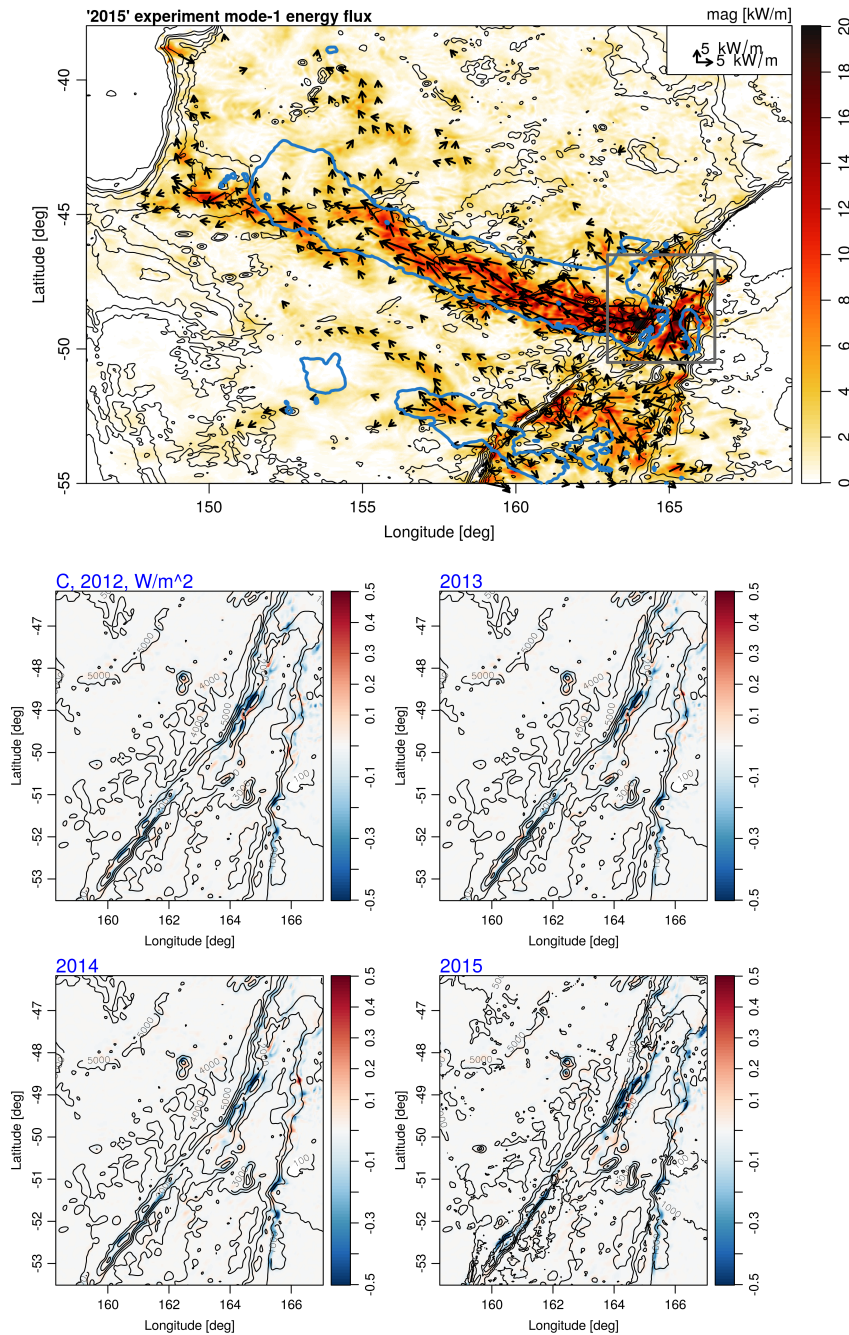


Figure 1: Energy flux map of the beam in Tasman Sea (a) and conversion rates at Macquarie Ridge (b).

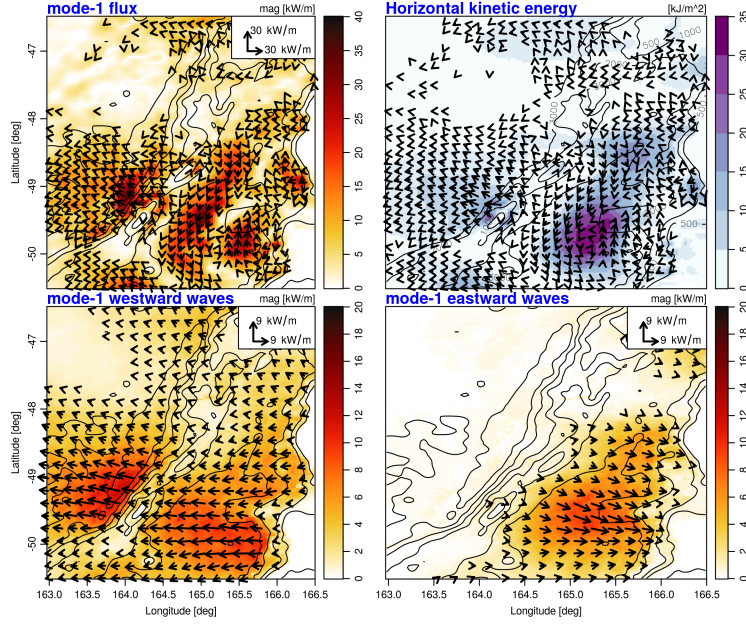


Figure 2: Standing wave

Spatial maps of conversion rates show variation in magnitude and location of conversion hotspots (Fig. 1). The energy transfers predominantly occur along steep flanks of two seamounts. The most striking difference was found between '2014' and 'uniform' experiment.

3.2 Variation of conversion rates and resonance

Conversion rates vary between experiments. Knife edge calculations with WKB-scaled depth does not confirm the same variations (Figure 2).

The other possibility for variations can be seen due to presence of remote waves. Model conversion rates and knife edge, Enhancement of generation due to remote propagating tides.

So variations in standing wave leads to variations in conversion.

3.3 Variation of Beam and its structure

The mid basin properties of the tidal beam include:

- wobbling
- slightly increased phase speed
- large deviations of group speed

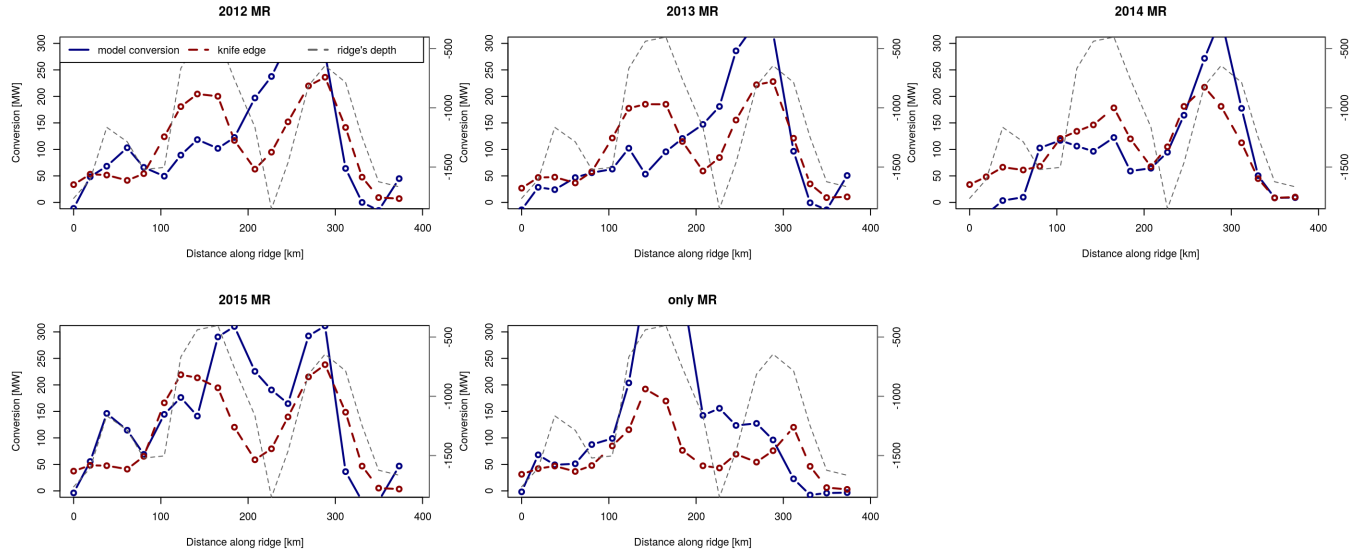


Figure 3: Variation of integrated conversion rates and knife edge

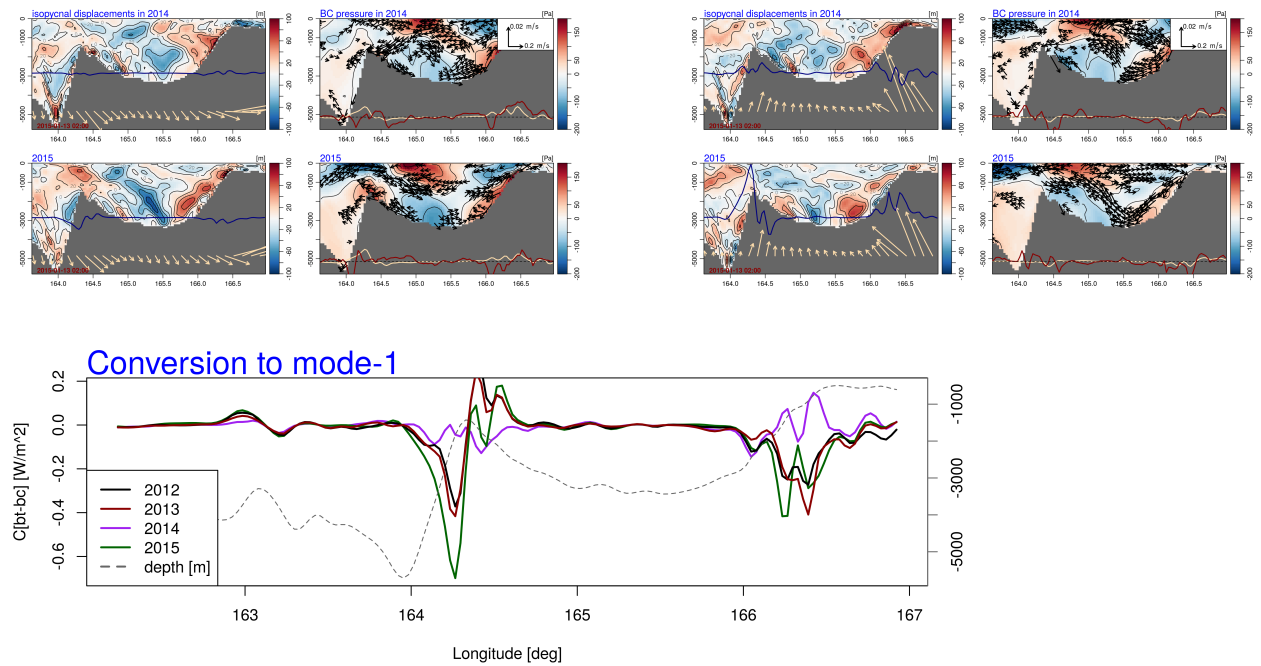


Figure 4: Model output

- wavefronts
- spotty APE and HKE

These properties point to use that the beam is a standing wave. But no apparent reflected wave is seen. Generation at Southern Tasman Plateau and Cascade Seamount can not be a source for opposite traveling waves due to their weakness. Additionally, directional spectra or plane wave fit does not show presence of such waves. But here we will show that generation indeed is responsible for wobbly pattern of the tidal beam and present a method that connects conversion pattern along Macquarie Ridge with mid basin characteristics of the beam.

4 Discussion

4.1 Variation of standing wave, HYCOM

We represent standing wave as interference of two waves (?),

Discussion on variability of standing wave: stratification?

It was tested hypothesis that the stratification controls, but results are inconclusive.

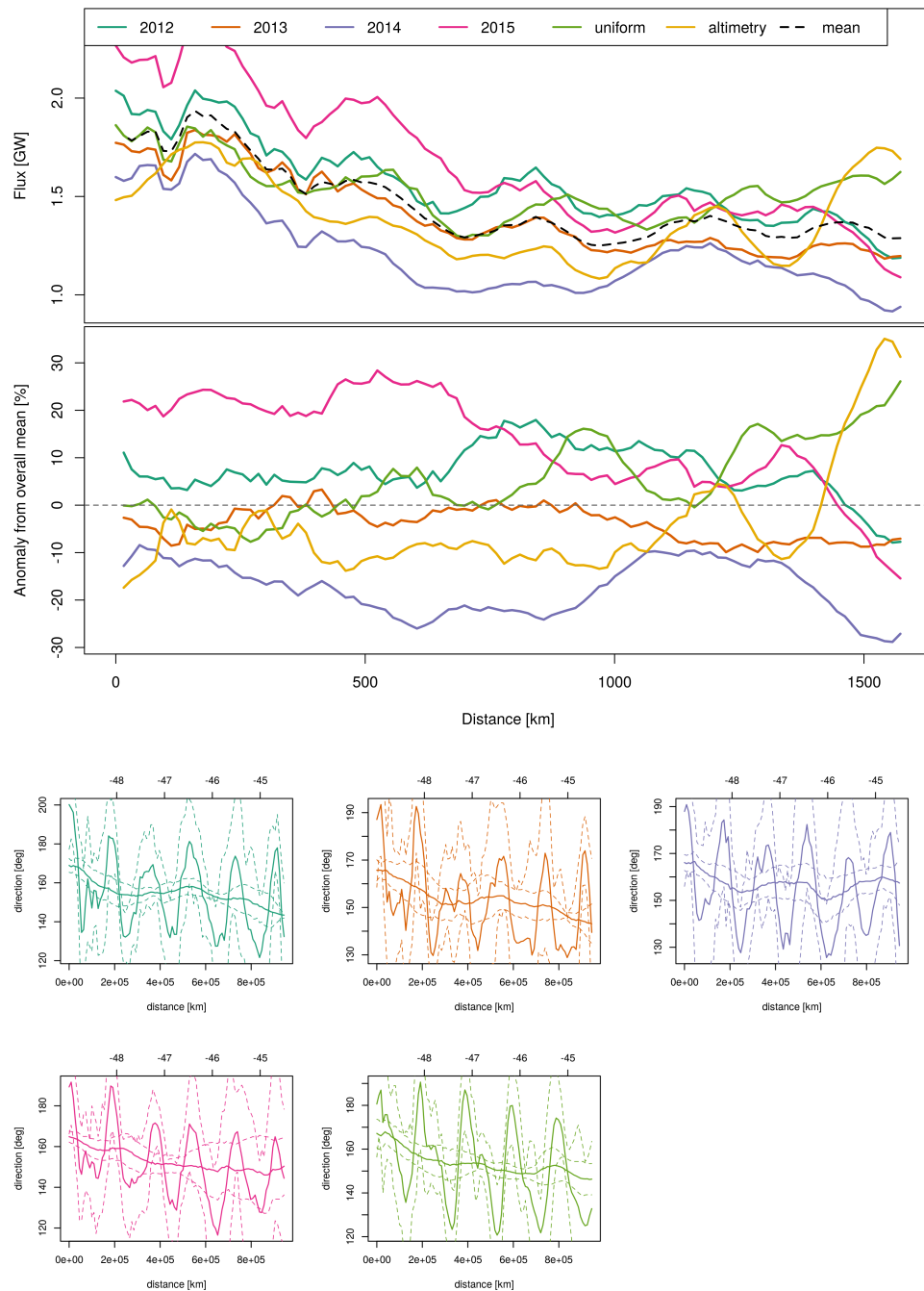
4.2 Inverse solution

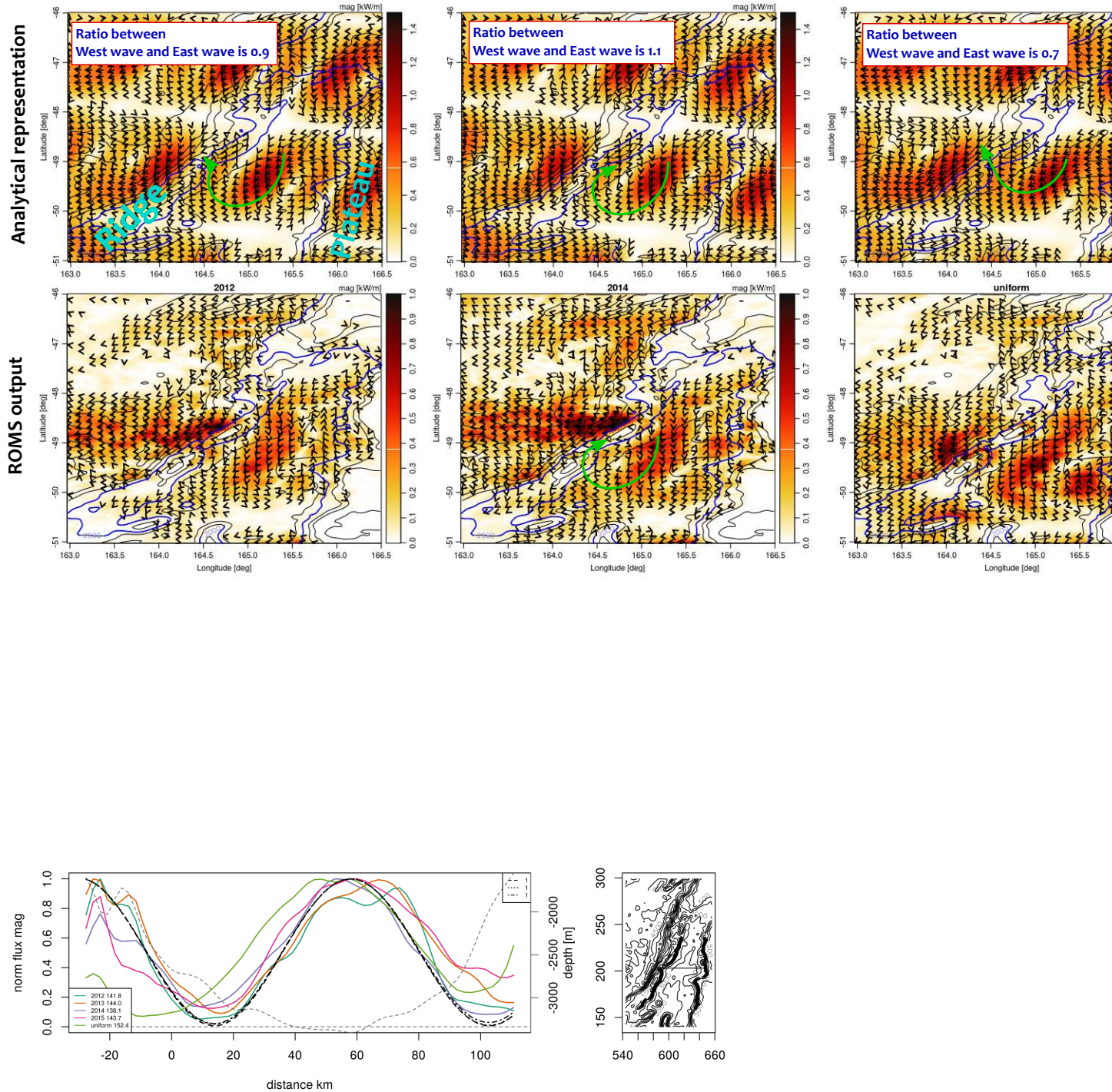
Study the wavefield varies depending on size of the ridge.

5 Conclusions

5.1 Generation in complex environment (Fabret-Perron)

5.2 Beam's stability





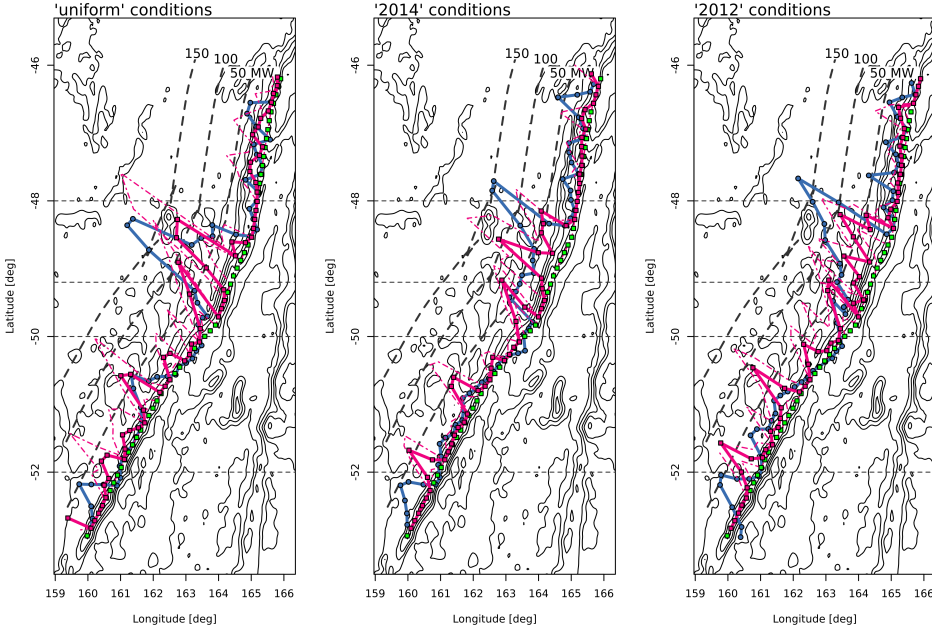


Figure 5: Comparison of inverse solution and numerically diagnosed.

A

Analytical solution

B

Analytical model for knife edge

Let consider a simplified problem of the internal tide generation at a three dimensional ridge. That is generating topography has extent in along x-axis, a , but infinitely small width. We will not pursue full solution of the problem and will not seek actual amplitudes of baroclinic modes, but rather concentrate on defining spatial pattern of the generated waves (might move up to opening). Under such problem statement the actual height is of no importance. And hence, in frame reference traveling with barotropic current, the topography becomes a piston-alike wavemaker that sends out the lowest mode internal tide. Its behavior in flat bottom ocean is well represented by Laplace tidal equations (cf Kelly et al. (2012)):

$$\vec{u}_t + 2\Omega \vec{k} \times \vec{u} = -\frac{1}{\rho_0} \nabla \cdot p \quad (4)$$

$$\nabla \cdot \vec{u} = -\left(\frac{1}{N^2 - \omega^2} p_z\right)_{tz} \quad (5)$$

with boundary conditions on the ridge,

$$\vec{u} \cdot \vec{n}|_{ridge} = \vec{u}_{bt} \cdot \vec{n}|_{ridge} \quad (6)$$

And boundary condition in the infinity implying outgoing waves. Note that barotropic current, in general, is given as a current ellipse written in complex form as $\vec{u}_{bt} = u_{bt} + iv_{bt}$.

This means that the boundary condition does not have a simple harmonic form. But the barotropic current can be decomposed to clockwise (CW) and counterclockwise components,

$$\vec{u}_{bt} = W_{CWE}e^{-(i\omega t - \phi_{CW})} + W_{CCWE}e^{(i\omega t + \phi_{CCW})} \quad (7)$$

and the generation of internal tide can be solved separately for two oppositely rotating currents. In further discussion the only one component (CCW) is taken care of since a solution will have similar form with differences arising in sign in front of tidal frequency. Considering rigid lid approximation and impermeable bottom equations for eigen modes is solved such that wavelength of corresponding mode is introduced. Then the dynamical equations can be reformulated as Helmholtz equation with harmonic temporal dependence implied and appropriate polarization relations,

$$\nabla^2 p + k_n^2 p = 0 \quad (8)$$

$$u = \frac{-i\omega p_x + fp_y}{\omega^2 - f^2}, \quad v = \frac{-i\omega p_y - fp_x}{\omega^2 - f^2} \quad (9)$$

Since the problem is now formulated in terms of pressure only, boundary condition takes the following form (Greenspan (1968)),

$$\left[\frac{-i\omega p_y - fp_x}{\omega^2 - f^2} \right]_{ridge} = \vec{u}_{BT}|_{ridge} \quad (10)$$

The above equations (5-8) state generation of internal tides by vibrating strip of width a . Such problem was solved for radiation of acoustic waves by Morse and Feshbach (1946). Since in Cartesian coordinates the strip boundary condition does not allow separation of variables, one can employ elliptic coordinate system,

$$x = \frac{a}{2} \cosh \mu \cos \theta, \quad y = \frac{a}{2} \sinh \mu \sin \theta$$

where edges of the strip will be focii of ellipse, boundary condition will take simpler form,

$$\left[\frac{-i\omega p_\mu + fp_\theta}{\omega^2 - f^2} \right]_{\mu=0} = \frac{a}{2} \sin \theta (\vec{u}_{BT}|_{\mu=0}) \quad (11)$$

The factor $\frac{a}{2} \sin \theta$ arises via conversion from Cartesian to elliptical derivatives. Note change of sign for p_{theta} because opposite growth of θ argument to x argument. Laplace operator in the elliptical coordinates has eigensolutions ("sloshing modes") in form of Mathieu functions (Stratton (2007)) that solution for the emitted waves will have form of,

$$p \sim \sum_j [Se_j, So_j](h, \theta) [Je_j, Jo_j, Ye_j, Yo_j](h, \mu) \quad (12)$$

with Se_j, So_j - angular Mathieu functions of order j corresponding to cos and sin, Je_j, Jo_j and Ye_j, Yo_j - radial Mathieu functions of the first and second kind of order j corresponding to Bessel functions. The physical parameter that sets Mathieu functions behavior is $h = ak_n 4$

so that in large distance limit, $h\mu \gg 1$, $rk_n \gg a$, they will represent circular harmonics. Now RHS of boundary condition (9) can be expressed in series of Mathieu functions,

$$\sin \theta = \sum_{j=0}^{\infty} C_{2j+1} So_{2j+1}(\theta) \quad (13)$$

with coefficients C_{2j+1} defined by normalization constants $N_{2j+1} = \int_0^{2\pi} So_{2j+1}^2(\theta) d\theta$ and the first Fourier coefficient of So_{2j+1} . The above series for sin and form of the boundary condition suggest solution in the form,

$$p(\mu, \theta) = \sum_{j=0}^{\infty} (A_{2j+1} So_{2j+1}(\theta) + B_{2j+1} Se_{2j+1}(\theta)) Ho_{2j+1}^1(\mu) \quad (14)$$

Here $Ho_{2j+1}^1(\mu) = Jo_{2j+1} + iYo_{2j+1}$ is a Hankel-Mathieu function. For CCW component to ensure condition for outgoing radiation, the sign should be different, so $Ho_{2j+1}^2(\mu) = Jo_{2j+1} - iYo_{2j+1}$.

Now substituting (11, 12) into (9) the unknown coefficients A , B are obtained,

$$(-i\omega(\sum ASo + BSe)Ho' + f(\sum ASO' + BSe')Ho) = \sum (\omega^2 - f^2)CSO$$

At first, multiplying above equation by So_{2m+1} and taking integral from 0 to 2π , so that $\int_0^{2\pi} So_{2m+1}Se_{2j+1}d\theta = \int_0^{2\pi} So'_{2j+1}So_{2m+1}d\theta = 0$, $\int_0^{2\pi} So_{2m+1}So_{2m+1}d\theta = No_{2m+1}$, $\int_0^{2\pi} So_{2m+1}Se'_{2j+1}d\theta = -N'_{2j+1}^{2m+1}$. In the last statement orthogonality between So and Se' is not satisfied. Equation on each order is obtained

$$(-i\omega A_{2m+1} No_{2m+1}^o Ho'_{2m+1} + f \sum_j B_{2j+1} Noe'^{2m+1}_{2j+1} Ho_{2j+1}) = CNo_{2m+1} \quad (15)$$

And at second, carrying out the same procedure but with Se_{2j+1} ,

$$(-i\omega B_{2m+1} Ne_{2m+1} Ho'_{2m+1} + f \sum_j A_{2j+1} Noe'^{2m+1}_{2j+1} Ho_{2j+1}) = 0 \quad (16)$$

Note that $\int_0^{2\pi} Se'_{2j+1} So_{2m+1}d\theta = -\int_0^{2\pi} So'_{2j+1} Se_{2m+1}d\theta$, i.e. $Noe'^{2m+1}_{2j+1} = -(Noe'^{2m+1}_{2j+1})^T$. Equations (13) and (14) form a linear system to find coefficients for different component of the total field. These equations are solved numerically with $j_{max} = 5$ due to rapid convergence of the involved series.

C Inverse model

The model closely follows ideas used in ref-to-Luc, 2010 and -Jody-2016. The internal tide generating ridge is given by point sources each emitting following

$$p = p_0 \frac{2}{\pi kd} \cdot e^{ikd} \quad (17)$$

where k - wavenumber associated with eigen mode-1, i.e. $k = \sqrt{\omega^2 - f^2}c_{eigen}^2$, d - distance between a point source and an observation point. By observation points here and after is meant points in which observations are inverted. The given solution is a solution of pressure disturbance propagation for two dimensional wave equation (p. 22, Frisk) and describes outgoing cylindrical wave. This is a far field approximation ($kd \ll 1$), in the near source zone the solution is substituted by Hankel functions. Here representation is simplified and observation points on the distance less than wavelength are omitted. Though introduction of Hankel function into the inverse model does not involve any additional complexity. By pressure here is thought mode-1 pressure amplitude that can be connected to sea level disturbance or isopycnal displacements.

To describe energy fluxes in the observational points polarization relations for cylindrical Poincare wave are invoked,

$$u = \frac{p_0}{\rho_{const}} * \frac{-i\omega \cos(\theta) + f \sin(\theta)}{\omega^2 - f^2} \cdot p_{\vec{d}} \quad (18)$$

$$v = \frac{p_0}{\rho_{const}} * \frac{-i\omega \sin(\theta) - f \cos(\theta)}{\omega^2 - f^2} \cdot p_{\vec{d}} \quad (19)$$

where $p_{\vec{d}}$ is a derivative along radius-vector \vec{d} ,

$$p_{\vec{d}} = (i \cdot k - \frac{1}{2d})p \quad (20)$$

In further description of the inverse model it is used following notation, indices i, k define i, k -th point sources, while j - j -th observation point.

The tidally and depth averaged energy fluxes will be given as an interference of pointwise fields from all sources,

$$F_j^x = \frac{1}{2} \sum_k u_{kj}^* \sum_i p_{ij} \int_H^0 \psi_1(z)^2 dz \quad (21)$$

$$F_j^y = \frac{1}{2} \sum_k v_{kj}^* \sum_i p_{ij} \int_H^0 \psi_1(z)^2 dz \quad (22)$$

Note different indexes for u/v and p meaning that cross multiplication is involved which leads to complex interference pattern. In energy flux formulation normalization coefficient associated with eigenmode structure function are introduced by corresponding mode-1 structure function, $\psi_1(z)$. Coefficient $1/2$ is used for convenience to convert actual time averaging involved to multiplication of complex numbers. In further description the constant coefficients are omitted due to their irrelevance. The previous relations can be expressed in matrix form (it is not fully correct for fluxes, multiplication is done term by term per point),

$$p_j = B_{ji}^p p_i, \quad u_j = B_{ji}^u p_i, \quad v_j = B_{ji}^v p_i \quad (23)$$

$$F_j^x = (B_{jk}^u p_k)^* B_{ji}^p p_i, \quad F_j^y = (B_{jk}^v p_k)^* B_{ji}^p p_i \quad (24)$$

where tensor notation is used, i.e. summation is done over same indices. Matrices B_{ij}^p , B_{ij}^u , B_{ij}^v are short notation for generation model and polarization relations, for example,

$$B_{ji}^p = p_i \frac{2}{\pi k d_j} \cdot e^{ikd_j} \quad (25)$$

These can be thought as discretization of operators transforming distribution of sources into interference pattern in pressure and velocity fields.

Apparently, the energy flux relations are non-linear. To deal with this it is proposed an iterative technique. Let at m -th iteration there is a known distribution of wave amplitude at sources, p_i^m , the total energy flux field can be reconstructed by (24). Than it is desired to find a small adjustment δp_i^m (“nudge factor”) such that residual between observed field and analytical description will be decreased. One can write,

$$\begin{aligned} F_j^x &= (B_{jk}^u(p_k^m + \delta p_k^m))^* B_{ji}^p(p_i^m + \delta p_i^m) = \\ &(B_{jk}^u p_k^m)^* B_{ji}^p p_i^m + (B_{jk}^u \delta p_k^m)^* B_{ji}^p p_i^m + (B_{jk}^u p_k^m)^* B_{ji}^p \delta p_i^m + (B_{jk}^u \delta p_k^m)^* B_{ji}^p \delta p_i^m \\ F_j^x - (B_{jk}^u p_k^m)^* B_{ji}^p p_i^m &= (B_{jk}^u \delta p_k^m)^* B_{ji}^p p_i^m + (B_{jk}^u p_k^m)^* B_{ji}^p \delta p_i^m + (B_{jk}^u \delta p_k^m)^* B_{ji}^p \delta p_i^m \end{aligned} \quad (26)$$

The left hand side of (26) represents the residual, the right hand side sets a controlling equation to obtain adjustment necessary to decrease the residual. The last term of RHS shows a non-linear nature of the problem. This is omitted since the purpose of consequent iterative technique is to find the final source distribution such that the model equations (24) are satisfied in least square sense. Than the “nudge-factor” can be found as inverse of

$$F_j^x - (B_{jk}^u p_k^m)^* B_{ji}^p p_i^m = R_j^x = \left[(B_{jk}^u)^* B_{ji}^p p_i^m + (B_{jk}^u p_k^m)^* B_{ji}^p \right] \delta p_i^m \quad (27)$$

(these equations are not in matrix form, but obsevation point by observation point). Hence, the aim of inverse model is to decrease error in representation of energy fluxes. The equation (27) can be solved separately for zonal and meridional fluxes and also simultaneously for both directions. That is at each iteration step the nudge-factor is found first for zonal, than for meridional direction and finally, for both simultaneously. At the end pressure distribution is changed by average from all three substeps.

Note the inverse model equation (27) is supported by additional condition stating that amplitude is nonnegative, $p_i^m + \delta p_i^m \geq 0$. All of this numerically is solved by linear programming routine lsei (least square with inequality) provided by LINPACK package.

D Convergence and Robustness

D.1 Description of the inverse model used in Tasman Sea studies

Here it will be presented a test convergence and number tests on robustness on proposed iterative inverse model. The initial flux field is given by Fig. 6 where by crosses are shown observational points. This define prescribed F_j^x or F_j^y . Note that the prescribed field aims to describe midbasin energy flux field with Tasman shelf ommitted due to presence of reflection and complex bathymetry. The point sources distribution are given by green dots and at the first iteration step are set to $p_i^0 = 100 \text{ Pa}$. The distribution of points sources is representative to distribution of steep bathymetry which is belived to be an internal tide generator. In the inverse model there are only two parameters that describe characteristic of the internal tide, wavenumber and normalization coefficients used in energy flux. Both are found from solving eigenvalue for randomly picked stratification profile. This result in wavelength of 180 km

which is a representative value for Tasman Sea conditions. In the same way eigenfunctions are obtained and normalization coefficients are found.

Hence, the inverse model does not account for

1. Bathymetry variation
2. Stratification variability
3. Variation of barotropic tide along ridges

The first two points are thought to have minor effect on internal tidal beam structure. While the third is omitted to preserve simplicity of generation model. Additional tests were done with variation in barotropic tide phase along ridges, but they did not bring any substantial changes in foregoing results.

To show convergence of the inverse model it is given change in pressure amplitude with each iteration. Here convergence is defined by

$$Conv = \sum_i \frac{(p_i^m - p_i^{m-1})^2}{(0.5 \cdot (p_i^m + p_i^{m-1}))^2}$$

The iterative solver is stopped when convergence is reaching tolerance. Here it is set to 0.01. From Figure (2a) it is seen that by 17th iteration there is no appreciable change in the inverse solution. This means that influence of non-linear terms in (26) became negligible and the distribution of amplitude along the source region is the best in least square sense. The error of such description is given on subsequent panels of Fig. 2, where root-mean-square-error for different energy flux parameters is defined for example zonal component as

$$E_x = \sqrt{\frac{\sum_{obs} (F_i^x - \hat{F}_i^x)^2}{N_{obs}}} \quad (28)$$

As it is seen the error is approaching stability for all used components much faster than convergence in amplitude. Note that the error is larger in zonal fluxes. The inverse solution can not predict far field behavior which is believed due to interaction with East Tasman Plateau. The obtained solution is given by Fig. 3. Here it is found that the inverse solution can not well represent the beam close to East Tasman Plateau. The following reasons can be named: interaction with topography and inadequacy of cylindrical wave model in the far-far field. It is believed that the second reason is the main. In general, the inverse solution picks up the central beam pretty well, outlines its boundary and the major region is satisfying manner. As well note that the northern and southern beams are also found in the solution.

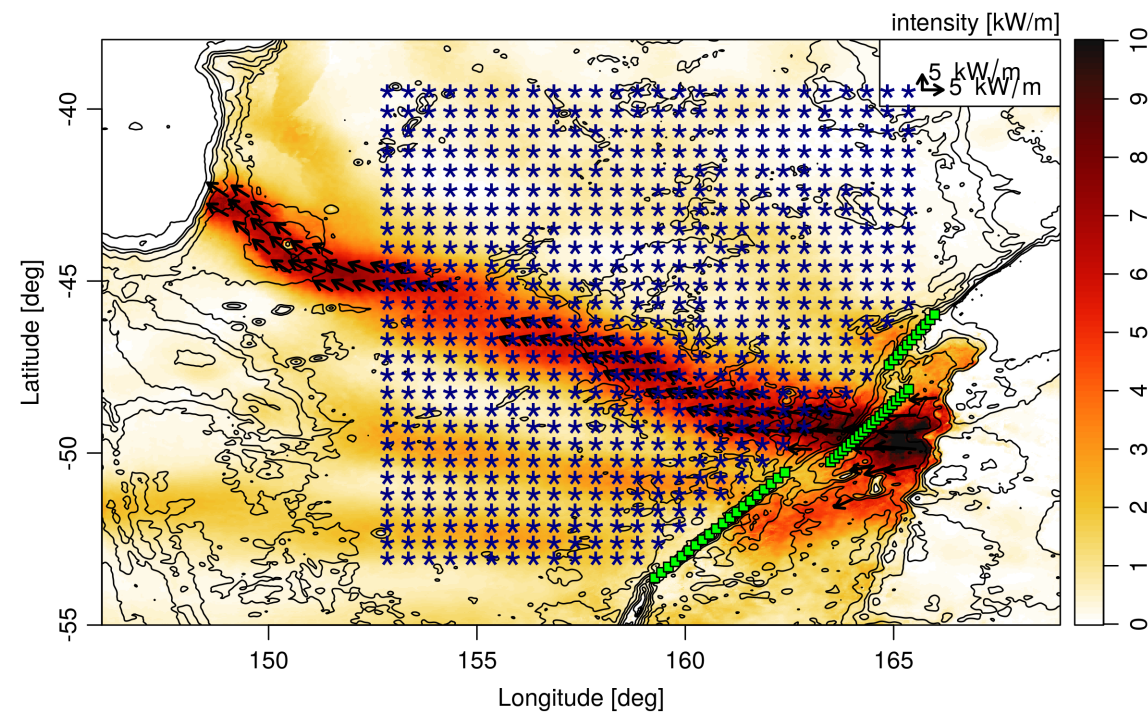


Figure 6: The input data (stars) and source model (green dots).

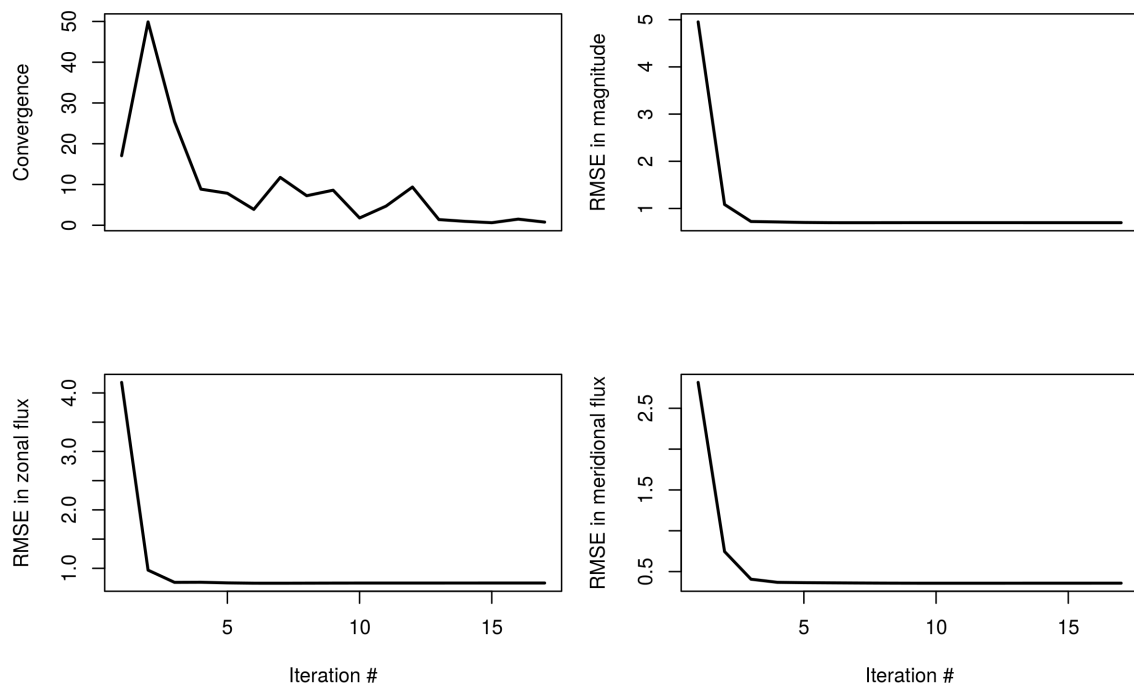


Figure 7: Convergence

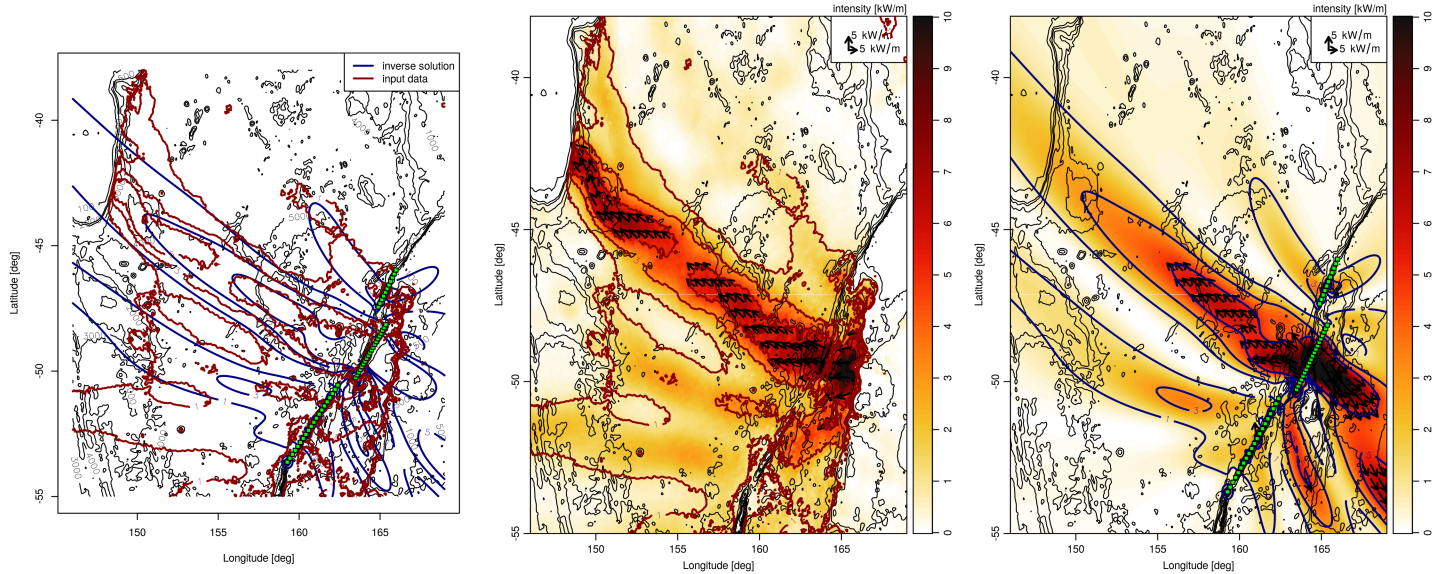


Figure 8: Left panel - Overlaid isolines of energy flux magnitude of magnitude 1, 3, 5 kW/m. Middle panel - input data. Right panel - inverse solution.

TO DO LIST

- Polish: Clin and energy budget, knife edge, WKB-stretching, standing wave
- Inverse model, elliptic waves are the way to go, why the phase can not be planar over much smaller stripes, something wrong with formulation of generation problem. See acoustics paper.
- Why in new experiments the beam did not move?
- Reasons for incoherence?
- Is there going to be any seasonal cycle?

References

- Ansong, J. K., Arbic, B. K., Alford, M. H., Buijsman, M. C., Shriver, J. F., Zhao, Z., Richman, J. G., Simmons, H. L., Timko, P. G., Wallcraft, A. J., et al. (2017). Semidiurnal internal tide energy fluxes and their variability in a global ocean model and moored observations. *Journal of Geophysical Research: Oceans*, 122(3):1882–1900.
- Buijsman, M., Uchiyama, Y., McWilliams, J., and Hill-Lindsay, C. (2012a). Modeling semidiurnal internal tide variability in the southern California bight. *Journal of Physical Oceanography*, 42(1):62–77.
- Buijsman, M. C., Klymak, J. M., Legg, S., Alford, M. H., Farmer, D., MacKinnon, J. A., Nash, J. D., Park, J.-H., Pickering, A., and Simmons, H. (2014). Three-dimensional

- double-ridge internal tide resonance in luzon strait. *Journal of Physical Oceanography*, 44(3):850–869.
- Buijsman, M. C., Legg, S., and Klymak, J. (2012b). Double-ridge internal tide interference and its effect on dissipation in luzon strait. *Journal of Physical Oceanography*, 42(8):1337–1356.
- Chavanne, C., Flament, P., Luther, D., and Gurgel, K. (2010). The surface expression of semidiurnal internal tides near a strong source at hawaii. part ii: Interactions with mesoscale currents*. *Journal of Physical Oceanography*, 40(6):1180–1200.
- Dunphy, M. and Lamb, K. G. (2014). Focusing and vertical mode scattering of the first mode internal tide by mesoscale eddy interaction. *Journal of Geophysical Research: Oceans*, 119(1):523–536.
- Dunphy, M., Ponte, A. L., Klein, P., and Le Gentil, S. (2017). Low-mode internal tide propagation in a turbulent eddy field. *Journal Of Physical Oceanography*, 47(3):649–665.
- Echeverri, P. and Peacock, T. (2010). Internal tide generation by arbitrary two-dimensional topography. *Journal of Fluid Mechanics*, 659:247–266.
- Egbert, G. and Ray, R. (2000). Significant dissipation of tidal energy in the deep ocean inferred from satellite altimeter data. *Nature*, 405(6788):775–778.
- Garrett, C. and Kunze, E. (2007). Internal tide generation in the deep ocean. *Annu. Rev. Fluid Mech.*, 39:57–87.
- Greenspan, H. P. (1968). *The theory of rotating fluids*. CUP Archive.
- Holloway, P. E. and Merrifield, M. A. (1999). Internal tide generation by seamounts, ridges, and islands. *Journal of Geophysical Research: Oceans*, 104(C11):25937–25951.
- Kelly, S. and Nash, J. (2010). Internal-tide generation and destruction by shoaling internal tides. *Geophysical Research Letters*, 37(23).
- Kelly, S. M., Nash, J. D., Martini, K. I., Alford, M. H., and Kunze, E. (2012). The cascade of tidal energy from low to high modes on a continental slope. *Journal of Physical Oceanography*, 42(7):1217–1232.
- Kerry, C. G., Powell, B. S., and Carter, G. S. (2013). Effects of remote generation sites on model estimates of m₂ internal tides in the philippine sea*. *Journal of Physical Oceanography*, 43(1):187–204.
- Kerry, C. G., Powell, B. S., and Carter, G. S. (2016). Quantifying the incoherent m₂ internal tide in the philippine sea. *Journal of Physical Oceanography*, 46(8):2483–2491.
- Morse, P. M. and Feshbach, H. (1946). *Methods of theoretical physics*. Technology Press.
- Munk, W. (1997). Once again: once againtidal friction. *Progress in Oceanography*, 40(1):7–35.

- Munroe, J. and Lamb, K. (2005). Topographic amplitude dependence of internal wave generation by tidal forcing over idealized three-dimensional topography. *Journal of Geophysical Research: Oceans*, 110(C2).
- Osborne, J., Kurapov, A., Egbert, G., and Kosro, P. (2011). Spatial and temporal variability of the m 2 internal tide generation and propagation on the oregon shelf. *Journal of Physical Oceanography*, 41(11):2037–2062.
- Pickering, A., Alford, M., Nash, J., Rainville, L., Buijsman, M., Ko, D. S., and Lim, B. (2015). Structure and variability of internal tides in luzon strait*. *Journal of Physical Oceanography*, 45(6):1574–1594.
- Rainville, L., Johnston, T. S., Carter, G. S., Merrifield, M. A., Pinkel, R., Worcester, P. F., and Dushaw, B. D. (2010). Interference pattern and propagation of the m 2 internal tide south of the hawaiian ridge. *Journal of Physical Oceanography*, 40(2):311–325.
- Stratton, J. A. (2007). *Electromagnetic theory*. John Wiley & Sons.
- Terker, S. R., Girton, J. B., Kunze, E., Klymak, J. M., and Pinkel, R. (2014). Observations of the internal tide on the california continental margin near monterey bay. *Continental Shelf Research*, 82:60–71.
- Wunsch, C. (1975). Internal tides in the ocean. *Reviews of Geophysics*, 13(1):167–182.
- Xing, J. and Davies, A. M. (1998). A three-dimensional model of internal tides on the malin-hebrides shelf and shelf edge. *Journal of Geophysical Research: Oceans*, 103(C12):27821–27847.
- Zaron, E. D. and Egbert, G. D. (2014). Time-variable refraction of the internal tide at the hawaiian ridge. *Journal of Physical Oceanography*, 44(2):538–557.
- Zhao, Z., Alford, M. H., Girton, J. B., Rainville, L., and Simmons, H. L. (2016). Global observations of open-ocean mode-1 m2 internal tides. *Journal of Physical Oceanography*, 46(6):1657–1684.
- Zilberman, N., Merrifield, M., Carter, G., Luther, D., Levine, M., and Boyd, T. J. (2011). Incoherent nature of m 2 internal tides at the hawaiian ridge. *Journal of Physical Oceanography*, 41(11):2021–2036.